ACS APPLIED MATERIALS & INTERFACES

LETTER

www.acsami.org

Tailored 3D Interface for Efficiency Improvement in Encapsulation-Free Hybrid Light-Emitting Diodes

Eugenia Martínez-Ferrero,*[,†,‡] Amparo Forneli,[†] Cédric Boissière,[§] David Grosso,[§] Clément Sanchez,[§] and Emilio Palomares[†,⊥]

[†]Institute of Chemical Research of Catalonia (ICIQ), Tarragona, Spain

[§]Laboratoire de Chimie de la Matière Condensée de Paris, UMR CNRS 7574, UPMC-Collège de France, Paris, France

[⊥]Institució Catalana de Recerca i Estudis Avançats (ICREA), Barcelona, Spain

Supporting Information

ABSTRACT: The modification of the planar organic/inorganic interface of the hybrid light-emitting diodes by the addition of a tailored nanoporous crystalline metal oxide increases up to 1 order of magnitude the efficiency of the resulting devices. In this Letter, we present the preparation and characterization of the novel controlled 3D interface and discuss how the interaction between the metal oxide and the polymer at the interface results in such an improvement.

KEYWORDS: light-emitting diodes, nanostructures, interface, electro-optical materials, metal oxides

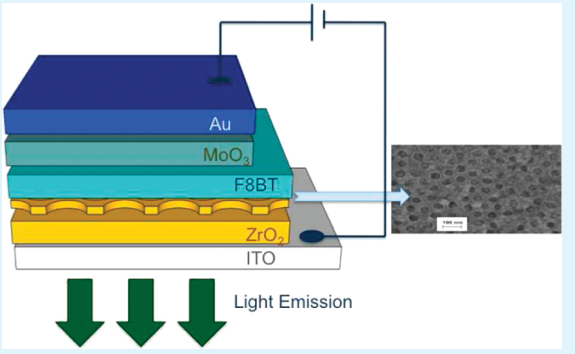

Hybrid organic−inorganic light-emitting diodes (HyLEDs) are novel devices with inverted organic LED structures that have proved ability to behave as competent LEDs with efficiencies comparable to Polymer LEDs.[1−3] Moreover, they involve low-cost metal oxides as charge transport layers that are much more stable under air operational conditions and can easily be combined with metallic high work function anode. Consequently, the devices do not require the hermetic encapsulation processes applied today to OLEDs,[4] lowering production costs and facilitating integration in buildings and large-scale applications for future outdoor lighting applications. However, the construction of efficient and commercial competitive light emitting hybrid devices must deal with the optimization of light emission and efficiency through the reduction of the exciton quenching and the decrease of the current density leakage at the organic/inorganic interface.

The typical structure of hybrid LED is made of an electron transport layer (ETL) deposited onto indium-doped tin oxide (ITO) cathode, followed by the successive deposition of the Light Emitting Polymer active layer (LEP), the hole transport layer (HTL), and finally the metallic anode. Transition metal oxides are often used as ETL (i.e., n-type like TiO_2 or ZnO) and HTL (i.e., MoO_3) because of their excellent robustness as well as for their chemical and physical characteristics. Briefly, electrons are injected through the ITO into the conduction band (CB) of the ETL, and into the lowest unoccupied molecular orbital (LUMO) of the LEP. However, this last step is not straightforward. The mismatch between the CB of the used metal oxide and the LUMO of most light emitting polymers results in a barrier for electron injection. Moreover, on the counter electrode, holes are injected through the metallic anode and through the MoO_3 layer, where because of the band alignment and the formation of an ohmic contact at the MoO_3/LEP interface,[5,6] they migrate much faster than the electrons toward the LEP/ETL interface. In addition, the mismatch between the metal oxide valence band (VB) and the highest occupied molecular orbital (HOMO) of the LEP impedes hole injection, resulting in the accumulation of positive charges at the ETL/LEP interface. Thus, charge transport in these devices is hole-dominated although much discussion is still arising to describe the device behavior using models. It is assumed that this built-up field enhances electron injection into the LEP despite the energetic barrier, and allows the subsequent electron−hole recombination. The decay of this excited state is accompanied by the emission of radiation whose frequency is the visible range.[7]

Therefore, the two main issues that need to be taken into account for the optimization of the efficiencies are: (i) the interfacial contact between the electrodes and the active layer, and (ii) the energy level alignment within the different components. The morphology at the ETL/LEP interface determines the device efficiency. For example, it has been observed that dense planar layers (i.e., TiO_2, ZnO) offer better results than their mesoporous equivalents despite the reduction of surface area since efficient charge injection requires an electric field that

Received: June 9, 2011
Accepted: August 1, 2011
Published: August 01, 2011

is maximized when using planar geometries.[8,9] In addition, polymer annealing enhances the interaction between the polymer and the ETL,[10] whereas thick polymer layers favor the formation of large recombination zones away from the interface, reducing the exciton quenching.[11] Second, the energy level alignment determines, with a precise correlative alignment, the injection rate and the turn-on voltages (Figure 2c). Several strategies have been followed to balance the charge transport and increase the electron injectiong rate alike the use of metal oxides with the CB above the LUMO of the polymer and deeper VB to block holes (i.e., using ZrO_2 as ETL), the use of Cs_2CO_3 derivatives as coatings on the ETL that n-dope the LEP, or the functionalization of the ETL surface with directional organic molecular dipoles or ionic liquid molecules to enhance electron injection.[12−15]

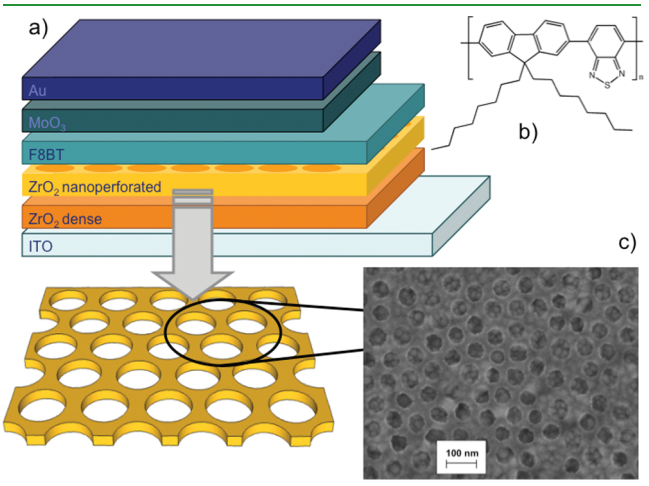

Figure 1. Illustration of the architecture of (a) HyLED device, and (b) the molecular structure of the LEP F8BT. (c) Top-view of the electron injection layer, shown on the FEG-SEM picture (magnification 250 Kx), displays the arrangement of the nanoperforations.

In this work, we show the improvement of the performance of HyLEDs through the construction of an electron transport layer made of a flat dense metal oxide layer, which maximizes charge recombination,[16] combined with a recent bottom-up method to create superficial nanoperforations onto this dense layer,[17] benefiting the morphology at the interface. Through this combination, we aim to address both issues at once, providing controlled and reproducible interfaces and tuning the energy level alignments for an enhanced electron injection. In addition, the present method involves low-cost sol−gel chemistry and dip-coating as liquid deposition process that is easy to scale up for prospective industrial applications.

First, a dense layer of ZrO_2 (addressed as Zr_d) has been deposited onto the ITO substrate, followed by the coverage by a second ZrO_2 layer (addressed as Zr_n) that is ultrathin (thickness <10 nm) and bears organized nanoperforations (Figure 1). The ordered array of nanoperforations was obtained by templating the sol−gel zirconia layer with block-copolymer micelles under specific conditions described in the Supporting Information. The characterization by FEG-SEM reveals the homogeneous distribution of uniform and circular nanoperforations, with average

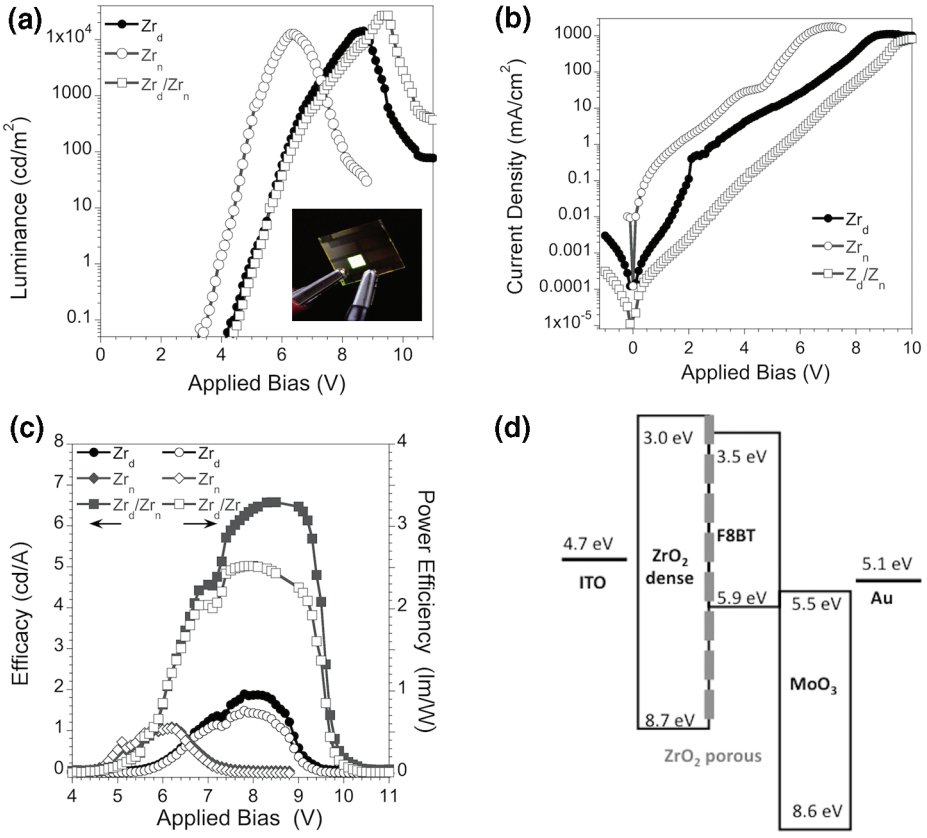

Figure 2. Performance of the Zr_d/Zr_n device compared to the device references Zr_d and Zr_n: (a) luminance versus applied bias, (b) current density versus applied bias, and (c) efficacy and power efficiency evolution with applied bias. Figure 2d shows the energy levels of the materials involved. The inset in panel a shows how the HyLED device works under ambient conditions without encapsulating layer.

Table 1. Electroluminescent Parameters Obtained for the Devices ITO/ZrO_2 Dense Layer/ZrO_2 Nanoperforated Layer/F8BT/MoO_3/ Au[a]

sample reference	Zr_d	Zr_d/Zr_n	Zr_n	BLANK[b]	OLED[c]
dense layer	ZrO_2	ZrO_2			
nanoperforated layer		ZrO_2	ZrO_2		
maximum luminance (cd m^{-2}) at voltage (V)	14200 (8.7)	25720 (9.4)[d]	11977 (6.6)	1500 (5)	1000 (8)
maximum efficacy (cd A^{-1}) at luminance (cd m^{-2})	1.8 (5055)	6.8 (4743)[d]	1.07 (11190)	0.08 (1360)	0.7
maximum power efficiency (lm W^{-1}) at luminance (cd m^{-2})	0.8 (5055)	2.9 (4743)[d]	0.5 (11190)	0.05 (1360)	0.6

[a] The results correspond to single devices that reflect the average performance of the different devices. The results reported in the literature for two blanks are also included for comparison purposes. [b] Structure ITO/F8BT/MoO_3/Au, results from ref 18. [c] Structure ITO/PEDOT:PSS/F8BT/Ba/Ag, results from ref 7. [d] Record values: 26890 cd m^{-2}, 13.8 cd A^{-1} and 4.6 lm W^{1-}.

diameters of 70 nm (Figure 1c), through which the surface of the underneath Zr_d layer is accessible, separated from center-to-center near neighbors by 90 nm. The AFM investigation (see Figure S1 in the Supporting Information), confirms that the so-called nanoperforations are cylinders of around 70 nm in diameter and reveals that they have an average depth of 6 ± 2 nm, in agreement with the 5 nm thickness measured by ellipsometry. From these data the areal density is estimated to be 1.2×10^{10} nanoperforations cm^{-2}, whereas the fraction of the accessible Zr_d surface was calculated to be 62 ± 5%. Consequently, the estimated increase in the surface area is 120 ± 5%. Subsequent to ETL preparation, the LEP F8BT (poly-9,9′-dioctyl fluorene-co-benzothiadiazole, Figure 1b) is deposited and annealed at 290 °C followed by the deposition of the counter electrode, resulting in devices of 0.09 cm^2 active area.

Light emission measurements, shown in Figure 2, illustrate the improved performance in every sample after addition of the Zr_n nanoperforated ultrathin layer. A record luminance of 26860 cd m^{-2} has been obtained with the latter Zr_d/Zr_n devices. Moreover, the best improvement is observed in current to light and power efficiencies pointing to the improved balance of the charge carrier transport. Figure 2 illustrates the benefit of the novel bilayer (Zr_d/Zr_n) device when compared to the single dense layer (Zr_d) device and to single nanoperforated ultrathin layer (Zr_n) device. The turn-on voltages for electroluminescence increase along with the complexity of the ETL: 3.1 V for the (Zr_n) device, 4.2 V for (Zr_d), and 4.5 V for (Zr_d/Zr_n), respectively. Taking into account that the workfunction of the electrodes and the energy levels of the materials involved in all the devices are similar (Figure 2d), we assign the shift of the turn-on voltage to the different thickness of the ETL (<8 nm for Zr_n, 17 nm for Zr_d, < 25 nm for Zr_d/Zr_n). The maximum luminance values follow the same trend, as well as the efficiency values (Figure 2c), which are inversely related to the current leakage. Figure 2b shows the variation of the current density with the applied bias. The (Zr_n) device displays the highest *J* values because the nanopores allow direct contact between the LEP and the ITO, consequently holes are not blocked and the current leakage increases. The dense layer in (Zr_d) decreases the number of charges reaching the ITO, and thus the current density values decrease in 1 order of magnitude. Finally, the combination of the nanoporous and the dense layers, (Zr_d/Zr_n), result in even lower current densities at similar applied bias. For example, at 8 V the current density is of 2000, 491, and 51 mA·cm^2 for (Zr_n), (Zr_d), and (Zr_n/Zr_d), respectively.

In this sense, the bilayer device (Zr_d/Zr_n) emits light more efficiently since, for the same applied bias, the power required to produce light is lower. Consequently, the parameter of efficiency is 1 order of magnitude higher than what is observed for both single-layer devices. Table 1 contains the results of single devices that reflect the average performance of the different devices. It must be noted that efficiencies of 13.8 cd·A^{-1} and 4.6 lm·W^{-1} have been reached in record devices whose luminance and current density evolution with applied bias are shown in Figure 2. The table also includes data of an F8BT-based OLED (structure ITO/PEDOT:PSS/F8BT/Ba/Ag)[7] and a blank device without ETL (structure ITO/F8BT/MoO_3/Au)[18] to provide a wider vision of the behavior of the devices. The charge injection scheme in the OLED is reversed and the holes are injected through the ITO while electrons are injected through the Ba/Ag electrode. The values obtained for both blanks are lower than those obtained for the devices with the Hyled approach, demonstrating the ability of the ZrO_2/F8BT interface to enhance electron injection and the hole blocking that turns out in higher efficiencies.

However, the enhancement of efficiency observed in the Zr devices is not proportional to the increase in the ETL thickness pointing to a better charge transport balance because of the presence of the nanoperforated layer at the ETL/LEP interface that increases the surface area. This leads to an extended area for injection as well as acting as a better hole-blocking layer through the increase of the thickness. In addition, the presence of the nanopores allows for an enhanced configuration of the polymer packing. It has been reported that F8BT polymer shows excellent electron transport in the parallel and perpendicular directions to the substrate.[19] Therefore, the nanopore cavities would provide an excellent pathway for electron injection into the polymer, and subsequent recombination with the holes accumulated in the polymer, reducing the number of charges reaching the electrodes. This fact is supported by the increase in luminance and the reduction of the current density at similar applied bias. Moreover, the surface properties of the materials at the nanometre scale depend on the ratio between the atoms on the surface and the atoms at the bulk,[20] and consequently, different structures made by the same material can show different properties. For example, the wettability of the surface is determined by the roughness and geometry of the layer.[21,22] On the other hand, the introduction of an organic polymer through the pores of mesoporous inorganic structures is an issue for the researchers due to the different hydrophilic nature of the two materials. Recently, it has been demonstrated that the alteration of the morphology of the inorganic metal oxide will assist the interaction between the organic and inorganic materials.[23] Similarly, the modification of the interface in hybrid solar cells has a deep effect on the performance of the device because of changes in the first few nanometers of the morphology of the polymer.[24] In this sense,

and taking into account the reduction of the current density reaching the counterelectrodes in the Zr_d/Zr_n devices, we can assume that a more intimate contact between the surface of the nanoperforated metal oxide and the polymer has been achieved, compared to the dense film, and due to the geometry of the nanopatterned layer. This enhanced morphology at the interface favors charge recombination that results in the enhanced luminance and the reduction of the charge density. It must be taken into account that in contrast to OLEDs,[25] light emission in HyLEDs follows a non-Lambertian pattern. This fact is due to the high refractive index of the ZrO_2 layer employed as ETL (n = 2.13) that causes optical wave-guiding. In this sense, because both layers are made of the same materials and because of the ultralow thickness of the Zr_n layer, we have discarded any light outcoupling effect on the final efficiency of the patterned device that could be originated from the Zr_n nanostructure. Therefore, we assume that the enhancement in the efficiency of the Zr_d/Zr_n devices arises from the moderate increase of surface area and, especially to the better packing of the polymer and the enhanced interaction between the polymer and the ETL promoted by the nanopores.

In conclusion, we have developed a tailored suprastructure for the ETL layer, which increases the interfacial surface area and leads to fine-tuning the electron injection into the LEP. The results presented in this work pave the way for overtaking the best-reported OLEDs efficiencies as well as for the applications requiring controlled nanotextured interfaces, hybrid devices, solar cells, transistors, and sensors.

■ ASSOCIATED CONTENT

Ⓢ Supporting Information. Description of the experimental procedure, AFM characterization of the film Zr_d/Zr_n, and performance of the (Zr_d/Zr_n) record device. This material is available free of charge via the Internet at http://pubs.acs.org.

■ AUTHOR INFORMATION

Corresponding Author
*E-mail: emartinez@cetemmsa.com.

Present Addresses
‡Currently at CETEMMSA, Mataró, Spain.

■ ACKNOWLEDGMENT

E.P. thanks the MICINN for the CONSOLIDER CDS-0007 HOPE-2007 and CTQ2010-18859 projects and the European Research Council for the ERC fellowship PolyDot. ICIQ and ICREA financial support is also gratefully acknowledged. E.M.-F. thanks the help of M. Faustini during the preparation of the metal oxide films, S. Borensztaj for the FEG-SEM measurements and M. Selmane for GISAXS measurements.

■ REFERENCES

(1) Bolink, H. J.; Brine, H.; Coronado, E.; Sessolo, M. *Adv. Mater.* **2010**, *22* (19), 2198–2201.
(2) Kabra, D.; Lu, L. P.; Song, M. H.; Snaith, H. J.; Friend, R. H. *Adv. Mater.* **2010**, *22* (29), 3194–3198.
(3) Sessolo, M.; Bolink, H. J. *Adv. Mater.* **2011**, *23* (16), 1829–1845.
(4) So, F.; Kondakov, D. *Adv. Mater.* **2010**, *22* (34), 3762–3777.
(5) Nakayama, Y.; Morii, K.; Suzuki, Y.; Machida, H.; Kera, S.; Ueno, N.; Kitagawa, H.; Noguchi, Y.; Ishii, H. *Adv. Funct. Mater.* **2009**, *19* (23), 3746–3752.
(6) Meyer, J.; Shu, A.; Kroger, M.; Kahn, A. *Appl. Phys. Lett.* **2010**, *96* (13), 133308.
(7) Bolink, H. J.; Coronado, E.; Repetto, D.; Sessolo, M.; Barea, E. M.; Bisquert, J.; Garcia-Belmonte, G.; Prochazka, J.; Kavan, L. *Adv. Funct. Mater.* **2008**, *18* (1), 145–150.
(8) Haque, S. A.; Koops, S.; Tokmoldin, N.; Durrant, J. R.; Huang, J.; Bradley, D. D. C.; Palomares, E. *Adv. Mater.* **2007**, *19* (5), 683–687.
(9) Kabra, D.; Song, M. H.; Wenger, B.; Friend, R. H.; Snaith, H. J. *Adv. Mater.* **2008**, *20* (18), 3447–3452.
(10) Bouclé, J.; Chyla, S.; Shaffer, M. S. P.; Durrant, J. R.; Bradley, D. D. C.; Nelson, J. *Adv. Funct. Mater.* **2008**, *18* (4), 622–633.
(11) Kabra, D.; Lu, L. P.; Song, M. H.; Snaith, H. J.; Friend, R. H. *Adv. Mater.* **2010**, *22* (29), 3194–3198.
(12) Tokmoldin, N.; Griffiths, N.; Bradley, D. D. C.; Haque, S. A. *Adv. Mater.* **2009**, *21* (34), 3475–3478.
(13) Morii, K.; Kawase, T.; Inoue, S. *Appl. Phys. Lett.* **2008**, *92* (21), 213304/1–213304/3.
(14) Park, J. S.; Lee, B. R.; Lee, J. M.; Kim, J.-S.; Kim, S. O.; Song, M. H. *Appl. Phys. Lett.* **2010**, *96* (24), 243306–3.
(15) Lee, B. R.; Choi, H.; SunPark, J.; Lee, H. J.; Kim, S. O.; Kim, J. Y.; Song, M. H. *J. Mater. Chem.* **2011**, *21* (7), 2051–2053.
(16) Morii, K.; Ishida, M.; Takashima, T.; Shimoda, T.; Wang, Q.; Nazeeruddin, M. K.; Gratzel, M. *Appl. Phys. Lett.* **2006**, *89* (18), 183510/1–183510/3.
(17) Kuemmel, M.; Allouche, J.; Nicole, L.; Boissiere, C.; Laberty, C.; Amenitsch, H.; Sanchez, C.; Grosso, D. *Chem. Mater.* **2007**, *19* (15), 3717–3725.
(18) Ryan, J. W.; Palomares, E.; Martinez-Ferrero, E. *J. Mater. Chem.* **2011**, *21*, 4774–4777.
(19) Donley, C. L.; Zaumseil, J.; Andreasen, J. W.; Nielsen, M. M.; Sirringhaus, H.; Friend, R. H.; Kim, J.-S. *J. Am. Chem. Soc.* **2005**, *127* (37), 12890–12899.
(20) Corma, A.; Atienzar, P.; Garcia, H.; Chane-Ching, J.-Y. *Nat. Mater.* **2004**, *3* (6), 394–397.
(21) Järn, M.; Brieler, F. J.; Kuemmel, M.; Grosso, D.; Lindén, M. *Chem. Mater.* **2008**, *20* (4), 1476–1483.
(22) Lee, W.; Park, B. G.; Kim, D. H.; Ahn, D. J.; Park, Y.; Lee, S. H.; Lee, K. B. *Langmuir* **2009**, *26* (3), 1412–1415.
(23) Baeten, L.; Conings, B.; Boyen, H.-G.; D'Haen, J.; Hardy, A.; D'Olieslaeger, M.; Manca, J. V.; Van Bael, M. K., *Adv. Mater.* **2011**, DOI:10.1002/adma.201100414.
(24) Lloyd, M. T.; Prasankumar, R. P.; Sinclair, M. B.; Mayer, A. C.; Olson, D. C.; Hsu, J. W. P. *J. Mater. Chem.* **2009**, *19* (26), 4609–4614.
(25) Greenham, N. C.; Friend, R. H.; Bradley, D. D. C. *Adv. Mater.* **1994**, *6* (6), 491–494.